Gamma emission in precompound reactions. II. Numerical application

M. Herman,[1] A. Höring,[2,3] and G. Reffo[1]
[1]*Ente Nazionale Energie Alternative, 40138 Bologna, Italy*
[2]*Max-Planck-Institut für Kernphysik, Heidelberg, Germany*
[3]*National Institute for Nuclear Theory, Seattle, Washington 98195*
(Received 6 July 1992)

The analytically obtained previous results on capture gamma ray reactions are used for a direct numerical calculation. It turns out that this formulation allows for a parameter-free description of gamma emission in precompound reactions. As an example we choose reactions induced by 14.1 MeV neutrons incident on ^{59}Co, ^{93}Nb, and ^{181}Ta. The individual contributions of different terms to the total cross section are discussed in detail and a comparison to experimental data is pursued.

PACS number(s): 24.10.−i, 24.60.Gv

I. INTRODUCTION

In the preceding paper [1] the gamma decay within preequilibrium nuclear reactions was formulated and calculated analytically by one of the present authors (A. H.) and by Weidenmüller. It is the goal of this sequel paper to numerically evaluate the analytically obtained expressions for the average S matrix and the average cross section. This enables us to compare our calculation to experimental data and other theoretical predictions. In the case of particle emission, such a program has recently been pursued by Herman, Reffo, and Weidenmüller [2]. Including the giant dipole resonance (GDR) into the description of preequilibrium nuclear reactions allows to account for the interdependence between GDR states and noncollective states in different exciton classes. This calls for a careful distinction of the different physical processes also in the numerical treatment. Thus, special care has to be taken in relating the analytically obtained expressions to numerically known quantities.

Throughout our numerical investigation the following assumptions are used: (i) The residual interaction is approximated by a two-body interaction. (ii) The GDR is treated as a doorway state with respect to the gamma channel only. Hence, the coupling to all other channels does not distinguish among GDR states and noncollective states in the same exciton class. (iii) Being a process of higher order the external coupling, i.e., the coupling among two exciton classes via a channel is neglected.

This paper is organized as follows. In Sec. II the input data for our numerical calculations, such as level densities, transmission coefficients, and average transition matrix elements between two exciton classes, are discussed. The semidirect (SD) and the multistep-compound (MSC) contributions to the cross section are investigated in Secs. III and IV, respectively. In Sec. V the precompound contribution, i.e., the MSC contribution modified by the SD contribution, is worked out. Our results are discussed in Sec. VI, and a brief summary is given in Sec. VII.

II. INPUT DATA FOR NUMERICAL CALCULATIONS

A. Average level density

The average level density for levels of exciton class N, $\rho_N(E,J,\pi)$, is given by the inverse average level spacing of the quasibound states with $(2N+1)$ excitons, energy E, spin J, and parity π. We assume that the spin and parity dependent part can be split off [4]:

$$\rho_N(E,J,\pi)=\frac{1}{2}\rho_N(E)\frac{(2J+1)}{2\sqrt{2\pi}\sigma_{(2N+1)}^3}\exp\left\{\frac{-(J+\frac{1}{2})^2}{2\sigma_{(2N+1)}^2}\right\}, \tag{2.1}$$

where σ_N is the spin-cutoff parameter. Using combinatorics $\rho_N(E)$ can be derived [4], yielding

$$\rho_N(E)=\rho(p,h,E) = \frac{g^{(p+h)}}{p!h!(N-1)!}\sum_{k=0}^{p}\sum_{l=0}^{h}(-1)^{k+l}\begin{bmatrix}p\\k\end{bmatrix}\begin{bmatrix}h\\l\end{bmatrix} \times\Theta(E-kB)(E-kB)^{N-1}, \tag{2.2}$$

where B is the difference of threshold energy of the one-body potential and the Fermi energy, p is the number of particles, and h the number of holes.

Since we restrict ourselves to a two-body residual interaction, the accessible state density, $\rho_{NJ\to MJ'}^{\rm acc}(E)$, is a useful tool. This level density is given by the average inverse level spacing of states in exciton class M with energy E and spin J' that are actually accessible starting from a state in exciton class N with spin J. This level density can also be derived using combinatorics. Here the expressions of Eqs. (12), (17), and (18) of Ref. [3] with corrections of Ref. [4] are used.

B. Transmissions coefficients

For the particle channels the transmission coefficients are derived using the optical model. We make use of the optical model parameters of Becchetti and Greenlees [5].

The transmission coefficients for the $E1$-gamma channel are defined like for the particle channel as the unitarity deficit of the average S matrix:

$$T_\gamma = 1 - \left| \overline{S_{\gamma\gamma}} \right|^2 . \tag{2.3}$$

This is directly proportional to the strength function $f(E)$, which itself can be written as a function of the absorption cross section, yielding

$$T_\gamma^{E1} = \frac{1}{2\pi} \sigma_{\rm abs}(E_\gamma^{E1}) \frac{(E_\gamma^{E1})^2}{(\hbar c)^2} . \tag{2.4}$$

The absorption cross section has a Lorentzian form and is given by

$$\sigma_{\rm abs}(E_\gamma^{E1}) = \sigma_{\rm res} \frac{(E_\gamma^{E1})^2 \Gamma_{\rm res}^2}{[(E_\gamma^{E1})^2 - E_{\rm res}^2]^2 + (E_\gamma^{E1})^2 \Gamma_{\rm res}^2} . \tag{2.5}$$

For the resonance energy $E_{\rm res}$, the resonance width $\Gamma_{\rm res}$, and the cross section in the resonance $\sigma_{\rm res}$, experimental data are used as input parameters.

C. Average coupling matrix element between noncollective states of two exciton classes

The average matrix element coupling noncollective states of two exciton classes can be determined from the imaginary part of the optical model potential. The spreading width of a particle is given by $2W(\epsilon)$, where $W(\epsilon)$ is the imaginary part of the optical model. To evaluate $\Gamma^{\downarrow}_{M\to(M+1)}$, $W(\epsilon)$ has to be averaged over the probability distribution of particles and holes. To avoid unnecessary duplication the interested reader is referred to [2] for further details.

III. MSC CONTRIBUTION TO THE CROSS SECTION

The pure MSC contribution to the cross section is obtained, neglecting the GDR built on the ground state. Thus all matrix elements including the GDR built on the ground state vanish. In this limit the average S matrix is diagonal, and the average cross section is given by

$$\overline{\sigma_{a,\gamma}^{\rm MSC}} = T_{a,Mm} \Pi_{Mm,Nn} T_{Nn,\gamma} , \tag{3.1}$$

where

$$(\Pi^{-1})_{Mm,Nn} = 2\pi\rho_{Mm} v^2_{Mm,Nn} 2\pi\rho_{Nn} + \delta_{M,N}\delta_{m,n} 2\pi\rho_{Mm} (\Gamma^{\uparrow}_{Mm} + \Gamma^{\downarrow}_{Mm}) \tag{3.2}$$

and $T_a = \sum_{Mm} T_{aMm}$ are the optical model transmission coefficients. As discussed in the introduction the external mixing has been neglected.

A. MSC matrix elements of the matrix Π

Since we use a two-body residual interaction, only neighboring exciton classes couple, i.e., $(\Pi^{-1})_{Mm,Nn} \neq 0$ only if $|M-N| \leq 1$. We analyze the individual matrix elements $(\Pi^{-1})_{Mm,Nn}$. We begin by investigating the nondiagonal block $(\Pi^{-1})_{Mm,(M+1)n} = 2\pi\rho_{Mm} v^2_{Mm,(M+1)n} 2\pi\rho_{(M+1)n}$, i.e., the transition from a state in exciton class M to a state in the next higher exciton class $(M+1)$. There are four different types of matrix elements: one type that describes the decay of a GDR, another type that describes its creation, still another type responsible for the single particle transitions leaving the GDR unchanged, and, finally, there are matrix elements that describe transitions among noncollective states. The question is how these matrix elements can be related to the numerically known quantities introduced in Sec. II. For this purpose, each type of matrix element is discussed individually. For illustration, the four possible transitions are sketched in Figs. 1(a)–1(d).

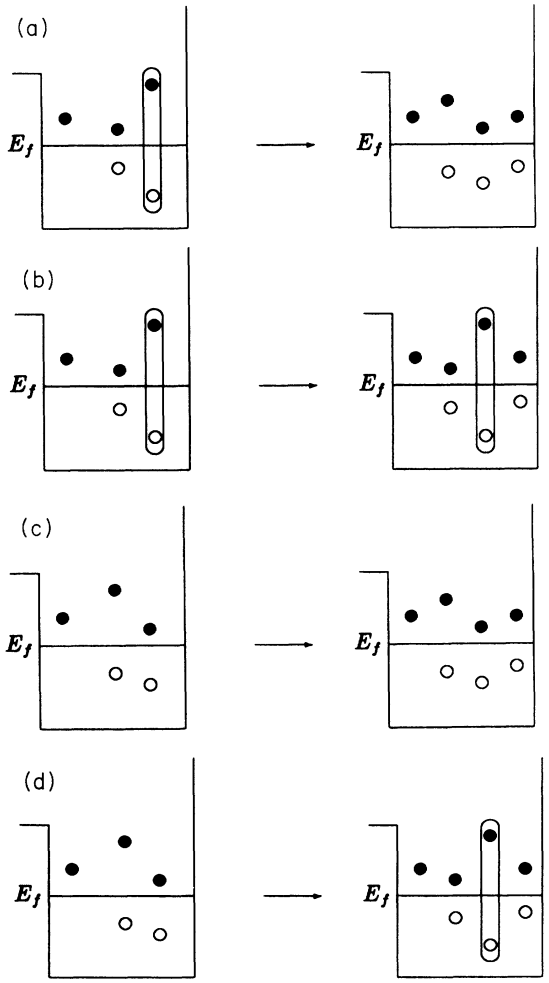

FIG. 1. (a) Sketch of the matrix element $(\Pi^{-1})_{Mm,(M+1)4}$, $m=1$, 2, or 3. (b) Sketch of the matrix element $(\Pi^{-1})_{Mm,(M+1)n}$, $m,n=1$, 2, or 3. (c) Sketch of the matrix element $(\Pi^{-1})_{M4,(M+1)4}$. (d) Sketch of the matrix element $(\Pi^{-1})_{M4,(M+1)m}$, $m=1$, 2, or 3.

The matrix element $(\Pi^{-1})_{Mm,(M+1)4}$, $m=1$, 2, or 3, describes the decay of a GDR via coupling to the next higher exciton class [cf. Fig. 1(a)]. This process is responsible for the spreading width of the GDR. This matrix element can be written as

$$2\pi\rho_{Mm}v^2_{Mm,(M+1)4}2\pi\rho_{(M+1)4}=2\pi\rho_{Mm}\Gamma^{\downarrow}_{\rm GDR}\ . \tag{3.3}$$

For the width of the GDR the experimental value is used. Unfortunately, there is little literature on how this width is separated into spreading and decay width. It is known that for heavy nuclei the spreading width is dominant, whereas for light nuclei the reverse is true. For ^{208}Pb approximately 90% of the width is due to the spreading width. For ^{16}O, on the other hand, 90% of the width is due to the decay width [6]. To separate the total width of the GDR into decay and spreading width, we assume a linear decay with $A^{1/3}$ for the decay width starting from 5 MeV in ^{16}O up to 0.5 MeV in ^{208}Pb [7]. As shown below in Sec. VI, our result depends only weakly on this assumption. For clarity, the angular momentum dependence of the level densities was not included in Eq. (3.3). Explicitly, the level densities $\rho^{J,\pi}_{Mm}(E)$ for $m=1,2,3$ are given by the exciton level densities $\rho^{(J-1),-\pi}_{M-1}(E-E_{\rm GDR})$, $\rho^{J,-\pi}_{M-1}(E-E_{\rm GDR})$, and $\rho^{(J+1),-\pi}_{M-1}(E-E_{\rm GDR})$, respectively. These correspond to the level densities of the noncollective states on which the GDR is built.

The matrix element $(\Pi^{-1})_{Mm,(M+1)n}$, $m,n=1,2,3$, describes the transition of a GDR state in class M to a GDR state in class $(M+1)$. This transition is sketched in Fig. 1(b). In such a transition the GDR is not affected and is just a "spectator." This is again a consequence of the two-body nature of the residual interaction. The subclasses 1,2,3 differ only in the angular momenta of the noncollective states the GDR is built on. Since a transition among these states must not change the angular momentum this part is diagonal in the subclass indices, i.e., $(\Pi^{-1})_{Mm,(M+1)m}\neq 0$, only. Thus, these matrix elements are given by

$$(\Pi^{-1})_{Mm,(M+1)m}=2\pi\rho_{Mm}v^2_{\rm n.c.}2\pi\rho^{\rm acc}_{Mm\to(M+1)m}\ , \tag{3.4}$$

where $\rho^{J}_{Mm}(E)$, $m=1,2,3$, is the exciton level density $\rho^{(J',-\pi)}_{M-1}(E-E_{\rm GDR})$ with $J'=(J-1),J,(J+1)$. $\rho^{\rm acc}_{Mm\to(M+1)m}(E)$, $m=1,2,3$, are the accessible state densities $\rho^{\rm acc}_{(M-1),J\to M,J'}(E-E_{\rm GDR})$ with $J'=(J-1),J,(J+1)$, respectively. $v_{\rm n.c.}$ stands for the average transition matrix element between two noncollective states of neighboring exciton classes. Only nonzero matrix elements are averaged.

The matrix element $(\Pi^{-1})_{M4,(M+1)4}$ describes transitions between noncollective states only [cf. Fig. 1(c)]. The matrix element is given by

$$(\Pi^{-1})_{M4,(M+1)4}=2\pi\rho_{M}(E)v^2_{\rm n.c.}2\pi\rho_{M\to(M+1)}(E)\ . \tag{3.5}$$

The matrix element $(\Pi^{-1})_{M4,(M+1)m}$, $m=1,2,3$, describes the creation of a GDR in the next higher exciton class [cf. Fig. 1(d)]. The Hamiltonian matrix elements that describe the creation of a GDR are identical with those that describe the decay of a GDR. However, the creation of a GDR is possible only if a particle or a hole has enough energy to create the GDR state. This is another consequence of the two-body nature of the residual interaction. A particle with the excitation energy of the GDR resonance energy generally is unbound. Thus, only a hole has a nonvanishing probability. The probability for a hole to have the energy ϵ with the total exciton number $(p+h)$ is given by

$$P(\epsilon)=N\frac{\rho(p,h-1,E-\epsilon)}{\rho(p,h,E)}\ , \tag{3.6}$$

where $\rho(p,h-1,E-\epsilon)$ is the level density of the remaining excitons—after removing a hole of the energy ϵ. $\rho(p,h,E)$ is the total level density at energy E for $(p+h)$ excitons. N is the normalization constant,

$$\frac{1}{N}=\int_0^E\frac{\rho(p,h-1,E-\epsilon)}{\rho(p,h,E)}d\epsilon\ . \tag{3.7}$$

The integrals are evaluated using Eqs. (12) and (13) of Ref. [4]. One obtains

$$\begin{aligned}\frac{1}{N}&=-\frac{\rho(p,h-1,E-\epsilon)}{\rho(p,h,E)(p+h-1)}\Bigg|_0^E\\&=\frac{\rho(p,h-1,E)}{\rho(p,h,E)(p+h-1)}\ .\end{aligned} \tag{3.8}$$

Hence, the probability for a hole to have the energy $E\geq E_{\rm GDR}$ is given by

$$\int_{E_{\rm GDR}}^E P(\epsilon)d\epsilon=\frac{(p+h-1)}{\rho(p,h-1,E)}\int_{E_{\rm GDR}}^E\rho(p,h-1,E-\epsilon)d\epsilon \tag{3.9}$$

$$=\frac{\rho(p,h-1,E-E_{\rm GDR})}{\rho(p,h,E)}\ . \tag{3.10}$$

Collecting everything yields

$$(\Pi^{-1})_{M4,(M+1)m}=2\pi\rho_{M4}(E)\Gamma^{\downarrow}_{\rm GDR}\frac{\rho(p,h-1,E-E_{\rm GDR})}{\rho(p,h,E)}\ . \tag{3.11}$$

Thus, all four types of matrix elements within the block $(M,M+1)$ have been determined. It remains to analyze the matrix elements of the blocks $(M+1,M)$ and (M,M).

The matrix element $(\Pi^{-1})_{(M+1)m,Mn}$ is obtained using the symmetry properties of the matrix Π^{-1}. The diagonal elements of this matrix can then be obtained by summation:

$$\begin{aligned}(\Pi^{-1})_{Mm,Mm}=&\sum_{n=1}^{4}(\Pi^{-1})_{Mm,(M+1)n}\\&+\sum_{n=1}^{4}(\Pi^{-1})_{Mm,(M-1)n}+\sum_c T_{Mm,c}\ .\end{aligned} \tag{3.12}$$

IV. SD CONTRIBUTION TO THE CROSS SECTION

Next, the contribution due to the average S-matrix element, $S_{a,\gamma}$, is investigated:

$$\left|\overline{S_{a\gamma}}\right|^2=\frac{2\pi W_{a0}^2}{(1+X_a)^2}\frac{1}{(E-E_0)^2+\frac{1}{4}\tilde{\Gamma}_0^2}\frac{2\pi W_{\gamma 0}^2}{(1+X_\gamma)^2}\ , \tag{4.1}$$

where

$$\tilde{\Gamma}_0=\sum_c\frac{2\pi W_{0c}^2}{1+X_c}+\sum_{Mm}v_{0,Mm}^2 2\pi\rho_{Mm}\ . \tag{4.2}$$

Again, we ask how this expression can be related to the quantities introduced in Sec. II in a way that is consistent with the precompound part of the cross section. The cross section (4.1) factorizes in three parts: $2\pi W_{a0}^2/(1+X_a)^2$ describing the coupling of the entrance channel a to the GDR built on the ground state, the propagator $1/[(E-E_0)^2+\frac{1}{4}\tilde{\Gamma}_0^2]$ and $2\pi W_{\gamma 0}^2/(1+X_\gamma)^2$ describing the gamma decay of the GDR. We will analyze each term individually. Multiplying numerator and denominator by $X_a=2\pi\sum_{Mm}v_{a,Mm}^2\rho_{Mm}$ we can rewrite the first term as

$$\frac{2\pi W_{a0}^2}{(1+X_a)^2}=\frac{X_a}{(1+X_a)^2}\frac{2\pi W_{a0}^2}{2\pi\sum_{Mm}v_{a,Mm}^2\rho_{Mm}}\ . \tag{4.3}$$

We recall that the transmission coefficient for a fixed channel a is given in microscopical terms by $T_a=4X_a/(1+X_a)^2$ [cf. Eq. (E5) in Appendix E of the preceding paper]. Due to the two-body nature of the residual interaction the entrance channel can only couple to the first exciton class. This removes the M summation. We assume the average Hamiltonian matrix element coupling channel a to the GDR build on the ground state to be equal to the matrix element coupling this channel to a noncollective state within the first exciton class. This is synonymous to the assumption that the GDR forms a doorway state with respect to the gamma channel only. In terms of the expressions introduced in Sec. II, this first part of the cross section is

$$\frac{2\pi W_{a0}^2}{(1+X_a)^2}=\frac{1}{4}\frac{T_a}{\rho_1}\ . \tag{4.4}$$

For the propagator the resonance energy, decay, and spreading width of the GDR are used. Again the decay width is modified by X_c which are determined from the respective transmission coefficient.

The term $2\pi W_{0\gamma}^2$ is the gamma decay width of the GDR. We stress, however, that it is not the total gamma decay width but rather the width for the gamma decay into a certain energy bin in order to obtain a spectrum. This can be expressed in terms of the transmission coefficients:

$$2\pi W_{0\gamma}^2 dE_\gamma^{E_1}=\frac{\rho(E-E_\gamma^{E_1},J_f,\pi_f)}{\rho(E,J_i,\pi_i)}T_\gamma(E_\gamma^{E_1})dE_\gamma^{E_1}\ . \tag{4.5}$$

V. PRECOMPOUND PART OF THE CROSS SECTION

In Sec. III we discussed the MSC part of the cross section. It is the goal of the present section to analyze the precompound part including the GDR built on the ground state. Neglecting external coupling, the latter part is given by [cf. Eqs. (4.5)–(4.8) of the preceding paper]

$$\overline{\sigma_{a,\gamma}^{fl}}=\sum_{MmNn}\left[(T_{a\gamma}T_{\gamma a})^{Mm,Nn}+(T_{aa}\tau T_{\gamma\gamma})^{Mm,Nn}\right]\Pi_{Mm,Nn}\ , \tag{5.1}$$

where

$$(\Pi^{-1})_{Mm,Nn}=-2\pi\rho_{Mm}v_{Mm,Nn}^2 2\pi\rho_{Nn}-2\pi\rho_{Mm}v_{Mm,0}^2\frac{1}{(E-E_0)^2+\frac{1}{4}\tilde{\Gamma}_0^2}v_{0,Nn}^2 2\pi\rho_{Nn}$$
$$+\delta_{M,N}\delta_{m,n}\left[2\pi\rho_{Mm}\Gamma_{Mm}^{\downarrow}+2\pi\rho_{Mm}v_{Mm,0}^2\frac{1}{(E-E_0)^2+\frac{1}{4}\tilde{\Gamma}_0^2}\left[\Gamma_0^{\downarrow}+2\pi\sum_c\frac{W_{0c}^2}{(1+X_c)^2}\right]\right.$$
$$\left.+\sum_c T_{Mm,c}\left[1-\frac{\frac{1}{2}\tilde{\Gamma}_0}{(E-E_0)^2+\frac{1}{4}\tilde{\Gamma}_0^2}\frac{2\pi W_{0c}^2}{(1+X_c)}\right]\right] \tag{5.2}$$

and

$$(T_{aa}T_{\gamma\gamma})^{Mm,Nn}=\left[T_{a,Mm}\left[1-\frac{\frac{1}{2}\tilde{\Gamma}_0}{(E-E_0)^2+\frac{1}{4}\tilde{\Gamma}_0^2}\frac{2\pi W_{a0}^2}{(1+X_a)}\right]+\frac{2\pi W_{a0}^2}{(1+X_a)^2}\frac{1}{(E-E_0)^2+\frac{1}{4}\tilde{\Gamma}_0^2}2\pi\rho_{Mm}v_{0,Mm}^2\right]$$
$$\times\left[T_{\gamma,Nn}\left[1-\frac{\frac{1}{2}\tilde{\Gamma}_0}{(E-E_0)^2+\frac{1}{4}\tilde{\Gamma}_0^2}\frac{2\pi W_{\gamma 0}^2}{(1+X_\gamma)}\right]+\frac{2\pi W_{\gamma 0}^2}{(1+X_\gamma)^2}\frac{1}{(E-E_0)^2+\frac{1}{4}\tilde{\Gamma}_0^2}2\pi\rho_{Nn}v_{0,Nn}^2\right]\ , \tag{5.3}$$

$$(T_{a\gamma}T_{\gamma a})^{Mm,Nn}=\frac{2\pi W_{a0}^2}{(1+X_a)^2}\frac{1}{[(E-E_0)^2+\frac{1}{4}\tilde{\Gamma}_0^2]^2}\frac{2\pi W_{\gamma 0}^2}{(1+X_\gamma)^2}$$
$$\times\left\{\left[2\pi\rho_{Mm}v_{0,Mm}^2+\frac{\tilde{\Gamma}_0}{2}\left[\frac{X_{a,Mm}}{1+X_a}+\frac{X_{\gamma,Mm}}{1+X_\gamma}\right]\right]\left[2\pi\rho_{Nn}v_{0,Nn}^2+\frac{\tilde{\Gamma}_0}{2}\left[\frac{X_{a,Nn}}{1+X_a}+\frac{X_{\gamma,Nn}}{1+X_\gamma}\right]\right]\right.$$
$$\left.+(E-E_0)^2\left[\frac{X_{a,Mm}}{1+X_a}-\frac{X_{\gamma,Mm}}{1+X_\gamma}\right]\left[\frac{X_{a,Nn}}{1+X_a}-\frac{X_{\gamma,Nn}}{1+X_\gamma}\right]\right\}. \tag{5.4}$$

Again the question is how to determine the terms not yet discussed using the expressions introduced in Sec. II. First, the terms in the matrix Π^{-1} are analyzed.

The expression $2\pi\rho_{Mm}v_{M,0}^2$ describes the coupling of states in class Mm to the GDR built on the ground state. Due to the two-body nature of the residual interaction, these elements have a nonvanishing contribution only for $M=2$. Depending on the subclass m, two types of these matrix elements need to be distinguished: for $m=4$ the coupling includes a noncollective state whereas for $m=1,2,3$ it is a transition including the GDR as a spectator. The former include the same matrix elements as for the GDR decay weighted with the probability for a hole having enough energy to create a GDR (cf. Sec. III). One obtains

$$2\pi\rho_{24}v_{2m,0}^2=\Gamma_0^{\downarrow}\frac{\rho_0}{\rho_{24}}\ . \tag{5.5}$$

The latter type, i.e., $m=1,2,3$, can be obtained as in Sec. III using the noncollective transition matrix element and the appropriate level densities. The propagator is the same as in the SD contribution analyzed in the preceding paragraph. The term $v_{0,MNn}^2 2\pi\rho_{Nn}$ describes the transition of the GDR built on the ground state to a state in class Nn. This term also vanishes for $N\neq 2$, and again there are two types of transitions depending on the subclass n. Both types are determined in the same way as the respective transitions discussed in detail in Sec. III.

The term

$$\frac{\tilde{\Gamma}_0}{(E-E_0)^2+\frac{1}{4}\tilde{\Gamma}_0^2}\frac{\pi W_{0c}^2}{(1+X_c)}$$

is of the order Λ^{-1}, where Λ stands for the number of channels. This becomes clear using the following argument. The largest contribution is obtained for $E=E_0$. $2\pi\sum_c W_{0c}^2$ is the decay width of the GDR and thus $\sum_c \pi W_{0c}^2/(1+X_c)\leq\Gamma_0^{\uparrow}/2<\Gamma_0$. Thus, the total expression summed over all channels is of the order of 1, and a single term is of the order Λ^{-1} and thus small compared to 1. This term was hence neglected.

Using (5.2) instead of (3.2) for the matrix Π^{-1} in Eq. (3.1) changes the value for the cross section only slightly. This change is six orders of magnitude smaller than the actual value of the cross section. This is due to the fact that all the terms of the matrix Π^{-1} discussed in this section are, like the external coupling via a channel, processes of higher order—the coupling of two classes via the doorway state.

The transmission coefficients are also modified due to the presence of the doorway state; cf. Eqs. (5.3) and (5.4). The individual terms can be rewritten using terms already discussed. This modification is again due to a higher order process, i.e., the coupling of a channel to a state in a specific exciton class via the doorway state. It turns out that also these modifications can be neglected.

VI. RESULTS AND DISCUSSION

We have calculated the (n,γ) cross section for neutrons with an incident energy of 14.1 MeV. As an exam-

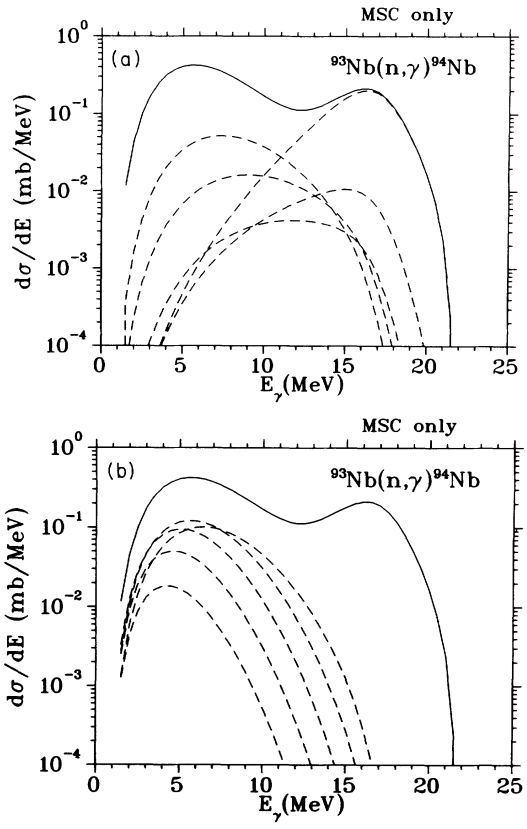

FIG. 2. (a) MSC spectrum for the reaction ^{93}Nb$(n,\gamma)^{94}$Nb, $E_n=14.1$ MeV. The dashed lines give the contribution of the decay of the exciton classes 2 through 6; the solid lines gives the total contribution. (b) MSC spectrum for the reaction ^{93}Nb$(n,\gamma)^{94}$Nb, $E_n=14.1$ MeV. The dashed lines give the contribution of the decay of the exciton classes 7 through 12; the solid line gives the total contribution.

ple, ^{93}Nb, ^{59}Co, and ^{181}Ta have been chosen as target nuclei to cover a large part of the periodic table. There exist experimental data for these target nuclei as well as theoretical predictions of other models allowing for a comparison. The parameters for the gamma absorption cross section have been taken from Ref. [8] for Ca and Ta and [9] for Na, respectively.

Figures 2–4 show the precompound gamma spectra for these nuclei. Only primary gamma emission was taken into account. The gamma emission from the individual classes is shown explicitly. The first three exciton classes[1] contributed to the GDR peak whereas the higher classes make up the compound nucleus peak. The peak energy moves to the left of the spectrum with growing exciton number. This is due to the fact that the cross section is weighted by the level density of the residual nu-

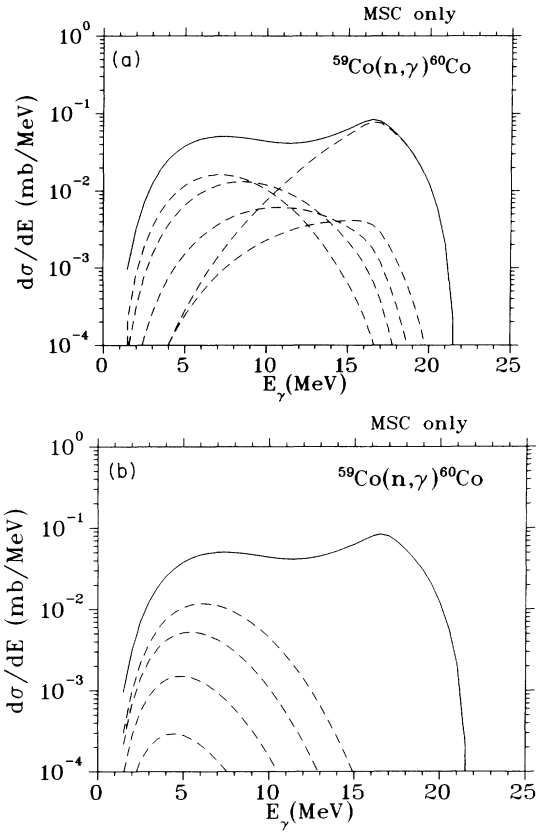

FIG. 3. (a) MSC spectrum for the reaction ^{59}Co$(n,\gamma)^{60}$Co, $E_n = 14.1$ MeV. The dashed lines give the contribution of the decay of the exciton classes 2 through 6; the solid line gives the total contribution. (b) MSC spectrum for the reaction ^{59}Co$(n,\gamma)^{60}$Co, $E_n = 14.1$ MeV. The dashed lines give the contribution of the decay of the exciton classes 7 through 12; the solid line gives the total contribution.

[1]They actually correspond to the exciton classes 2 through 4, since the first exciton class makes a gamma decay via the SD process only.

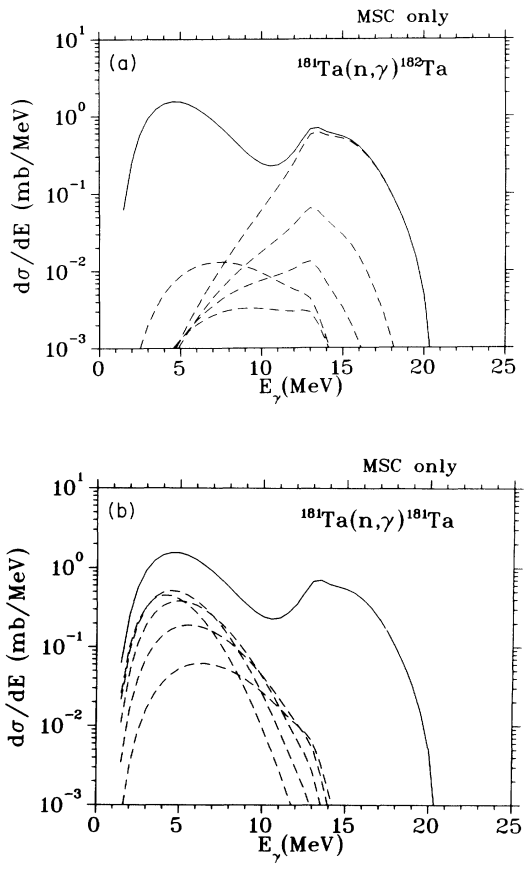

FIG. 4. (a) MSC spectrum for the reaction ^{181}Ta$(n,\gamma)^{182}$Ta, $E_n = 14.1$ MeV. The dashed lines give the contribution of the decay of the exciton classes 2 through 6; the solid line gives the total contribution. (b) MSC spectrum for the reaction ^{181}Ta$(n,\gamma)^{182}$Ta, $E_n = 14.1$ MeV. The dashed lines give the contribution for the decay of the exciton classes 7 through 12; the solid line gives the total contribution.

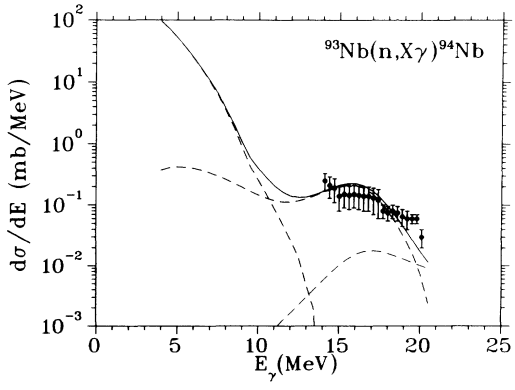

FIG. 5. Total gamma spectrum for the reaction ^{93}Nb$(n,\gamma)^{94}$Nb, $E_n = 14.1$ MeV (solid line). The dashed lines give the MSC and the SD contributions of the (n,γ) reaction and the contribution of the $(n,n'\gamma)$ reaction, respectively. The experimental data were taken from [10].

cleus. The latter grows with the excitation energy. The growth increases with exciton number.

Comparison of such a spectrum with a typical spectrum for particle emission, e.g., for a (n,n') reaction, shows that both spectra are similar in shape. In the case of particle emission, too, the higher exciton classes tend to be responsible for the compound nucleus peak, whereas the first few exciton classes create a peak at a higher energy in the spectrum. The latter is not as strongly pronounced as it is in the case of gamma emission. The difference lies in the E^4 dependence of the transmission coefficient for the gamma channel. Also, the absolute value of the two cross sections is very different. In the case of particle emission, the second peak is of the order of a few hundred mb. On the other hand, in the case of gamma emission the latter is of the order a few hundred μb.

Figures 5–7 show the total gamma spectrum as a sum of the SD contribution, the precompound contribution, and the gamma emission after emission of a neutron, i.e., $(n,n'\gamma)$. The latter was treated by a Hauser-Feshbach calculation. For a complete description of the gamma spectrum, the contribution of the $(n,2n\gamma)$ and of the $(n,p\gamma)$ reactions should also be considered. This yields an even steeper exponential falloff at small energies. For a comparison, experimental data have also been plotted. These data were taken from Refs. [10] and [11]. Comparison of our predictions with these experimental data shows nice agreement without the need of any free parameters. For Nb and Ta our calculations predict slightly higher values than observed experimentally whereas for Co we obtain slightly smaller results. It should be mentioned that our result depends very sensitively on the GDR parameter, i.e., the absorption cross section. If, for example, the GDR parameters for Nb had also been used for Co, the theoretical predictions in the Co case would also have been slightly higher than the experimentally observed data. Furthermore, different experiments yield different results for the gamma absorption cross section.

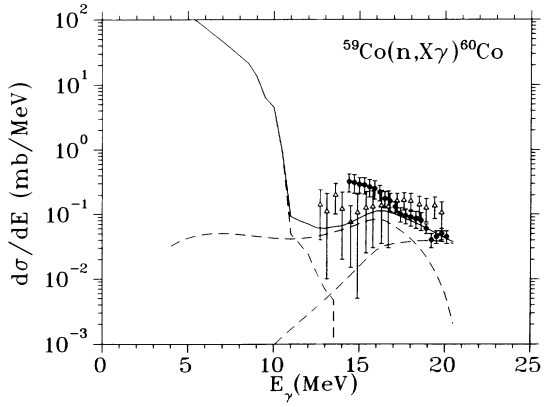

FIG. 6. Total gamma spectrum for the reaction ^{59}Co$(n,\gamma)^{60}$Co, $E_n = 14.1$ MeV (solid line). The dashed lines give the MSC and the SD contributions of the (n,γ) reaction and the contribution of the $(n,n'\gamma)$ reaction, respectively. The experimental data were taken from [10] (●) and [11] (△), respectively.

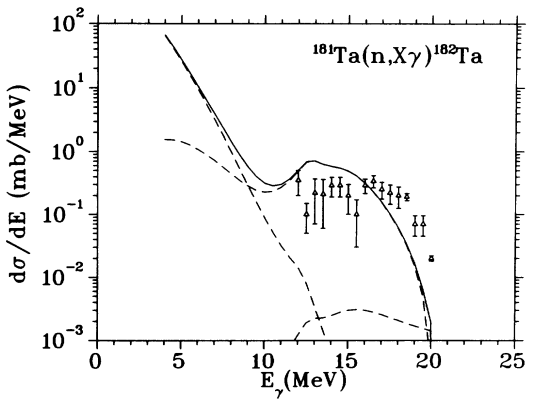

FIG. 7. Total gamma spectrum for the reaction ^{181}Ta$(n,\gamma)^{182}$Ta, $E_n = 14.1$ MeV (solid line). The dashed lines give the MSC and the SD contributions of the (n,γ) reaction and the contribution of the $(n,n'\gamma)$ reaction, respectively. The experimental data were taken from [11].

In all three cases, the SD part of the cross section is small compared to its MSC part. A major reason is the terms X_a appearing in the SD part. These terms take into account the possible coupling of the channels to the noncollective states. This causes the flux that couples the channel to the GDR built on the ground state to be reduced. For illustration, Fig. 8 shows the SD cross section for $X_a = 0$. Our numerical approach to the SD term is very different to conventional DSD calculations, where the individual matrix elements are calculated microscopically. This makes a comparison of the two theories doing justice to both difficult. Our motivation has not been to reproduce existing DSD calculations but merely to use a consistent numerical treatment for all different physical processes discussed earlier. We thereby limit ourselves to only using the input data discussed in Sec. II to avoid using free parameters.

In Table I we examine the dependence of our results on the relation $\Gamma_0^{\downarrow}/\Gamma_0$ using Nb as an example. The form of

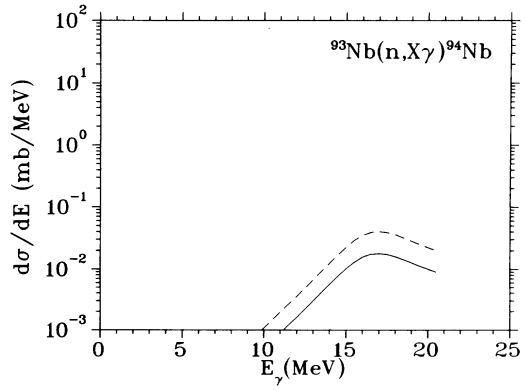

FIG. 8. SD gamma spectrum for the reaction ^{93}Nb$(n,\gamma)^{94}$Nb, $E_n = 14.1$ MeV. The solid line gives again our result. The dashed line shows this spectrum for $X_a = 0$ for a comparison.

TABLE I. MSC- and SD-peak cross section in μb for the reaction ^{93}Nb$(n,\gamma)^{94}$Nb as a function of the ratio $\Gamma_0^{\downarrow}/\Gamma_0$.

$\Gamma_0^{\downarrow}/\Gamma_0$	σ^{SD} (μb)	σ^{MSC+SD} (μb)
0.1	19.4	276
0.2	19.2	273
0.3	19.0	265
0.4	18.8	257
0.5	18.6	248
0.6	18.5	241
0.7	18.3	233
0.8	18.0	226
0.9	17.9	220
1.0	17.7	214

the cross section is not changed but the variation of this ratio affects only the absolute value of the spectrum. Hence, it suffices to analyze the value of the SD and the precompound cross section in the peak as a function of this ratio. With increasing $\Gamma_0^{\downarrow}$ and thus decreasing $\Gamma_0^{\uparrow}$, it becomes more likely for the GDR to decay into a more complex state than into a channel. This explains the monotone decrease of the cross section as a function of this ratio. It also turns out that our result depends only weakly on this ratio, especially in the realistic regime that lies for Nb between 60% and 80%.

Since it is experimentally relatively easy to create 14.1 MeV neutrons most of the experimental data for neutron-induced reactions are taken using 14.1 MeV neutrons. Our theoretical description, however, is not restricted to this energy. Nonetheless, it is sensible to choose the energy of the projectile in this regime since there the preequilibrium contribution is largest. For a much smaller incident energy it becomes unrealistic to excite the GDR. On the other hand, if the incident energy is much larger the cross section is dominated by direct reactions. For high incident energies it is very likely that the residual nucleus after emitting a photon is left in a continuum state which is not treated in this model.

Our calculations can be carried out for any nucleus for which such a statistical treatment is justified provided the gamma-absorption cross section is known. Thus, our model can make predictions.

VII. SUMMARY

The results of the preceding paper [1] were applied to numerically calculate the total (n,γ) cross section for 14.1 MeV incident neutron energy. As an example ^{59}Co, ^{93}Nb, and ^{181}Ta were chosen as target nuclei. We formulated the results derived in [1] in terms of numerically known quantities such as the absorption cross section, level densities, and optical model transmission coefficients. This shows that practical calculations within a fully quantum mechanical theory are feasible and allow for a parameter-free description of such processes. It turns out that this description is in good agreement with the experimental data and is valid for all nuclei through the periodic table where such a theoretical description is justified (cf. [1]).

However, our numerical treatment can still be improved. We are currently investigating the effect of using more realistic level densities calculated in a large shell model space. Especially for the smaller exciton classes this could yield a major improvement. This would particularly improve our result for the SD contribution.

In this sense, we view this paper as a step towards a physically sound approach being able to treat consistently all major mechanisms leading to gamma emission.

ACKNOWLEDGMENTS

We are grateful to F. S. Dietrich and H. A. Weidenmüller for helpful discussions. We also thank H. A. Weidenmüller for a careful reading of the manuscript. One of us (A.H.) wishes to thank M. Herman and G. Reffo for their kind hospitality. We thank the Department of Energy for partial support during the completion of this work.

[1] A. Höring and H. A. Weidenmüller, Phys. Rev. C **46**, 2476 (1992), the preceding paper.
[2] M. Herman, G. Reffo, and H. A. Weidenmüller, Nucl. Phys. **A536**, 124 (1992).
[3] K. Stankiewicz, A. Marcinkowski, and M. Herman, Nucl. Phys. **A435**, 67 (1985).
[4] P. Obložinský, Nucl. Phys. **A453**, 127 (1986).
[5] F. D. Becchetti and G. W. Greenlees, Phys. Rev. **182**, 1190 (1969).
[6] G. F. Bertsch, P. F. Bortignon, and R. A. Broglia, Rev. Mod. Phys. **55**, 287 (1983).
[7] G. F. Bertsch, private communication.
[8] S. S. Dietrich and B. L. Berman, At. Data Nucl. Data Tables **38**, 199 (1988).
[9] H. Gruppelaar and P. Nagel, NEA Data Bank–Newsletter Nr. 32, Gif-sur-Yvette, France (1985).
[10] F. Rigaud, J. L. Irigaray, G. Y. Petit, G. Longo, and F. Saporetti, Nucl. Phys. **A173**, 551 (1971).
[11] M. Budnar *et al.*, International Atomic Energy Agency Report INDC(YUG)-6/L, 1979.